ADVANCED MATERIALS TECHNOLOGIES
www.advmattechnol.de

Multi-Material Gradient Printing Using Meniscus-enabled Projection Stereolithography (MAPS)

*Puskal Kunwar, Arun Poudel, Ujjwal Aryal, Rui Xie, Zachary J. Geffert, Haven Wittmann, Daniel Fougnier, Tsung Hsing Chiang, Mathew M. Maye, Zhen Li, and Pranav Soman**

Light-based additive manufacturing methods are widely used to print high-resolution 3D structures for applications in tissue engineering, soft robotics, photonics, and microfluidics, among others. Despite this progress, multi-material printing with these methods remains challenging due to constraints associated with hardware modifications, control systems, cross-contamination, waste, and resin properties. Here, a new printing platform coined Meniscus-enabled Projection Stereolithography (MAPS) is reported, a vat-free method that relies on generating and maintaining a resin meniscus between a crosslinked structure and bottom window to print lateral, vertical, discrete, or gradient multi-material 3D structures with no waste and user-defined mixing between layers. MAPS is compatible with a wide range of resins shown and can print complex multi-material 3D structures without requiring specialized hardware, software, or complex washing protocols. MAPS's ability to print structures with microscale variations in mechanical stiffness, opacity, surface energy, cell densities, and magnetic properties provides a generic method to make advanced materials for a broad range of applications.

1. Introduction

Current additive manufacturing methods are unable to match nature's marvelous ability to arrange multiple materials in 3D configurations across scales to realize multifunctional structures.[1–5] Extrusion or jetting methods with the use of multiple printing nozzles have been used to print multi-material structures, however, the print resolution, surface finish, shape fidelity, and speed are typically lower than vat photo-polymerization methods such as Projection stereolithography (PSLA) or digital light processing (DLP).[6–8] A typical setup for PSLA consists of spatially modulated light patterns projected through a transparent bottom window to polymerize photosensitive liquid resin in a vat.[9–11] The ever-growing library of resin formulations has already allowed PSLA to fabricate functional structures for applications in tissue engineering, soft robotics, photonics, and other fields.[12–18] Despite this progress, multi-material printing with PSLA or similar methods remains challenging due to limits of hardware modifications, complex control systems, resin properties, and associated constraints as explained below.

Advances in PSLA technology such as continuous liquid interface production (CLIP), high-area rapid printing (HARP), and computed axial lithography (CAL), have improved printing speed, however, their ability to print multiple materials remains limited.[19–21] Current multi-material PSLA methods continue to rely on proprietary hardware modifications such as the use of multiple vats, carousel-style rotators, linear movement of print stages, wiping mechanisms, and pressurized fluid flow to facilitate resin exchanges.[17,22–28] Instead of relying on passive refilling of resins, lateral (XY) stage motion in mask video projection-based stereolithography (MVP-SL)[29] has been used to accelerate rapid refilling of resins, however, this requires customized hardware and control modifications. Active perfusion of resin using viaducts embedded within the print geometry (Injection CLIP or iCLIP), has also been used to accelerate the refilling of resins.[29,30] However, the embedded viaduct geometry itself induces artifacts to the printed construct. Multi-material printing with CAL, which relies on the projection of light patterns onto a rotating resin vat, is possible only when the second material is printed around pre-existing prints. Recently reported

P. Kunwar, A. Poudel, U. Aryal, R. Xie, Z. J. Geffert, H. Wittmann, D. Fougnier, P. Soman
Biomedical, and Chemical Engineering Department
Syracuse University
Syracuse, NY 13210, USA
E-mail: psoman@syr.edu
P. Kunwar, A. Poudel, U. Aryal, R. Xie, Z. J. Geffert, H. Wittmann, D. Fougnier, P. Soman
BioInspired Institute
Syracuse, NY 13210, USA
T. H. Chiang, M. M. Maye
Department of Chemistry
Syracuse University
Syracuse, NY 13210, USA
Z. Li
Department of Mechanical Engineering
Clemson University
Clemson, SC 29634, USA

The ORCID identification number(s) for the author(s) of this article can be found under https://doi.org/10.1002/admt.202400675

DOI: 10.1002/admt.202400675

DLP-based centrifugal multi-material (CM) method involves lifting the stage out of the vat and applying centrifugal forces to clean resin residues from previous prints before re-immersing it back into the vat to print a second material; this requires hardware modifications and is limited to discrete multi-material printing.[31] Other strategies of greyscale light exposure or orthogonal dual-wavelength printing require customized resin photochemistry and/or complex optical engineering setups.[32]

Additionally, resin properties continue to play a dominant role in determining the printing capabilities of current methods. For instance, resins that are miscible with the lubricating liquid, necessary for rapid printing, cannot be used with HARP.[25] The DLP-based CM method is limited to materials that could withstand the centrifugal washing steps while CAL is limited to resins that exhibit high viscosity, high reactivity, and low scattering properties.[31] Vat-free techniques such as 3D printing from a single droplet have been demonstrated to continuously print 3D structures from a single drop of resin.[33] In another example, puddles of resins or smaller droplets with lateral or vertical stage movements, have also been used, although challenges related to separation forces between glass and polymerized parts, air-cleaning of high viscosity resins, and flow of large puddles remain.[34] In summary, despite recent advances, current multi-material PSLA methods require hardware and software modifications, and key challenges related to resin refilling, contaminations during resin exchanges, and low recyclability due to unpredictable amounts of photoreactive components have not been addressed. These limitations become even more challenging for gradient printing, as generating consistent and accurate material transitions within the printed object becomes difficult due to issues like residue buildup and cross-contamination. These factors hinder the ability to precisely manipulate the resin's properties required for successful gradient printing, emphasizing the need for new methods to overcome these challenges.[35]

In this work, we report the design and development of a Meniscus-enabled Projection Stereolithography or MAPS platform. As compared to conventional methods, MAPS is a vat-free method that is capable of printing 3D structures with custom variations in lateral, vertical, discrete, or gradient properties with minimum waste and contamination. To demonstrate its broad utility, MAPS was used to print 3D structures with custom variations in stiffness, opacity, surface energy, cell density, and magnetic properties.

2. Result and Discussion

2.1. MAPS

Conventional stereolithography methods rely on a resin reservoir or vat to additively crosslink layers with programmed stage movements. As compared to vat-based methods, MAPS relies on the generation and continuous maintenance of a resin meniscus between crosslinked layers and the bottom PDMS window (**Figure 1A**; Figure S1, Supporting Information). When a resin droplet is placed onto a cured polydimethylsiloxane (PDMS) surface, the resin tends to form a dome across the surface and form a three-phase contact line between the liquid resin, the solid PDMS surface, and the surrounding air. The behavior of this three-phase contact line is influenced by the surface tension of the liquid resin, and interfacial tensions at the resin–air and PDMS–resin boundaries. The surface tension of resin is characterized by the contact angle $\theta 1$, the angle between a tangent to the liquid resin's surface and the adjacent solid surface (Figure 1A(i)). As the print starts and progresses, the newly crosslinked layers lead to the formation of another 3-phase contact line between resin, crosslinked layers, and air and are defined by contact angle ($\theta 2$) (Figure 1A(ii)). This, in essence, leads to the formation of a resin meniscus (Figure 1A(iii)), which serves as a reservoir for the MAPS printing process.

A 405 nm light, spatially modulated via a digital micromirror device (DMD) and projected through the PDMS bottom window, is used to crosslink liquid resin in a layer-by-layer manner (Figure S1-S2, Supporting Information). Vertical stage movement generates negative pressure which continuously draws the resin from the meniscus toward the fabrication window (light projected area on PDMS) against adhesion forces between resin and PDMS and between resin and crosslinked layers. As the printing process continues, a fluidic pump supplies new resin and maintains the meniscus throughout the printing process (Figure 1A). Ideally, the resin consumption and replenishment rates should be identical to generate minimum waste or cross-contamination in the case of multi-material printing. This involves adjusting the flow rate based on the volume of resin needed for each layer during the printing process, a process that is explained in detail in the supporting information (Section S4, Supporting Information). Modular use of multiple infusion ports, syringe pumps, and inline micromixers, allows easy and rapid configuration of the system for printing customized multi-material structures.

In MAPS, the oxygen permeability of the PDMS window facilitates the generation of a "dead zone" just above the fabrication window to prevent unwanted adhesion of newly crosslinked layers to the bottom window during the printing process. (Figure S1A, Supporting Information). It is worth noting that the dead zone is a thin layer with uncrosslinked polymer between the PDMS slab and the cross-linked structure, where polymerization doesn't occur effectively due to oxygen inhibition. Oxygen diffuses through the permeable PDMS window and interferes with the cross-linking of the polymer, which prevents the newly cross-linked layers from adhering to the bottom window.[2,21] For a particular resin formulation and CAD design, the upward stage movement was coordinated with layer exposure times, dead-zone thickness, light dosage per layer, and the fluidic flow rate of new resin. Before multi-material printing, model resin PEGDA 400 MW was used to quantify lateral and axial resolution of MAPS using a "line array" and "staircase" templates respectively. The desired layer thickness (50 μm, for PEGDA 400) was generated by programming the stage to move up (200 μm) and down (150 μm) during light irradiation. (Figure 1B(i–iv)). With PEGDA 400 resin, lateral and axial resolutions were quantified as 10.05 ± 0.7 μm and 42.79 ± 1.12 μm respectively. For vertical resolution experiments, the PEGDA resin was mixed with 1% (2-Isopropylthioxanthone (ITX) (photosensitizer) and 0.25% Irgacure 819 (photoinitiator) to achieve a range of axial feature sizes ranging from 42.79 ± 1.12 to 122.24 ± 4.45 μm using exposure times varying from 0.5–2 s per layer (Figure 1C(i–iv)). The precision of the printing was evaluated by calculating the coefficient of variation (CV). This assessment of variability yielded values of 6.7% for lateral resolution and 2.61% for axial resolution,

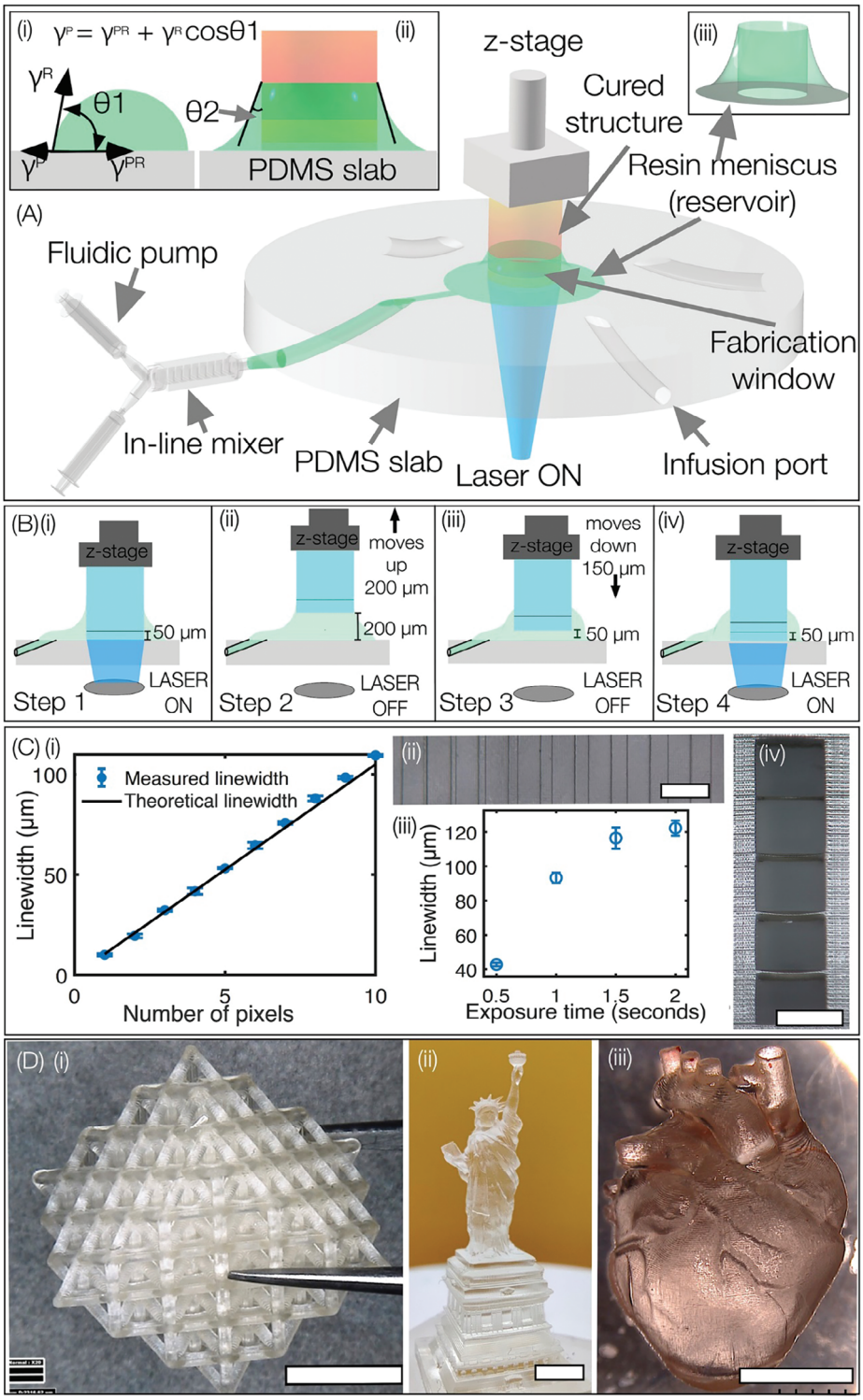

Figure 1. A) Schematic setup illustrating the MAPS 3D printing by a continuous flow of resin solution using syringe pumps and an inline micromixer. i) Formation of the three-phase contact line and resin shape dictated by γ^R – resin surface tension, γ^P- PDMS surface tension, γ^{PR} – resin-PDMS boundary tension, and contact angles $\theta 1$ and $\theta 2$. ii) Illustration of contact angle $\theta 2$ once the structure starts to print. iii) Shape of the meniscus that acts as a reservoir for MAPS printing. B) i–iv) Process flow diagram of steps involved in MAPS. The programmed up-down motion of the z-stage draws the liquid into the fabrication area, while the projection of spatially patterned 405 nm light crosslinks the resin solution. (C) Plots and photographs showing i, ii) lateral resolution (scale bar-200 µm) and iii, iv) axial resolutions (scale bar – 500 µm) of printed structure using model resin PEGDA 400 MW. For error bars in i, iii), mean ± SD ($n = 3$) (D) i) Lattice cube ii) the Statue of Liberty and iii) the human heart structures fabricated using MAPS. (scale bar – 3 mm).

indicating the capacity of MAPS to generate high-resolution 3D structures with minimal deviation from the specified parameters. The above-mentioned formulation of PEGDA 400 was used to print a "lattice cube", "Statue of Liberty", and "human heart" structures using a layer thickness of 50 μm, a laser intensity of 3.25 mW cm^{-2}, and an exposure time of 0.7 s per layer. The printed structure was washed and developed in an ethanol solution for 5 min. (Figure 1D(i–iii); Video S1, Supplementary Video). Several commercially available resins such as B9Creations Black resin, PhotoCentric 3D grey, Liqcreate Flexible-X, Liqcreate Composite-X, Siraya Tech Blu, and Siraya Tech Sculpt were also tested (Figure S6, Supporting Information). Details related to resin formulation and associated printing conditions can be found in Table S1 (Supporting Information). It is worth noting that MAPS utilizes a programmed discrete up-and-down movement of the stage for each layer before the photocrosslinking step. For instance, when the target layer thickness is 50 μm, the stage moves upward by 200 μm and then descends by 150 μm for low viscous resins, while for highly viscous resins such as eResin-Elastic from eSUN, the stage moves upward by 1 mm and descended 950 μm. This discrete up-and-down strategy counteracts surface adhesion forces, facilitates the drawing of new resin to the fabrication window, and makes MAPS compatible with a wide range of resin viscosities. Overall, these results demonstrate the capability of MAPS to effectively print 3D structures with resolutions at par with other VAT-based methods.

2.2. Optimization of MAPS for Multi-Material and Gradient Printing

Printing multi-material discrete and gradient structures with minimum waste or minimum cross-contamination between layers requires the presence of minimal meniscus volume in the fabrication area. (**Figure 2A**). During the printing process, the contact angle that a particular resin formulation makes with PDMS changes continuously. A larger contact angle or an excess resin in the fabrication window leads to a higher degree of mixing between crosslinked layers, while lower contact angles or insufficient resin in the fabrication window leads to a disruption of resin transport from the inlet port to the meniscus and generates defects. Thus, to ensure an uninterrupted and contamination-free printing process, new resin, ideally exactly equal to the resin needed for crosslinking the next layer, needs to be transported to the meniscus throughout the printing process. To study how the contact angle between resin and PDMS influences the MAPS process, we developed a new multiphase many-body dissipative particle dynamics (mDPD) model. (Figure 2B; Video S2, Supplementary Video). The setup shows the fabrication window (between z-stage printhead size, D = 5 mm), PDMS window, and infusion port (Dt = 0.5 mm). Results for different substrate wetting contact angles ($\theta 1$ = 20°, 45°, 90°, and 110°) showed that when the substrate becomes more hydrophilic, liquid adhesion is increased, resulting in the spreading of the droplet onto a wider wetting area. On the other hand, increased hydrophobicity of the substrate ($\theta 1$ = 110°) weakens liquid adhesion and makes it more susceptible to liquid-bridge breakage at a location between the printhead and pump outlet. Multiphase fluid simulations provided valuable insight into the underlying physics of multiphase flow and droplet wetting. For instance, we identified an ideal contact angle range (30°–45°) that would prevent any disruptions in resin flow from the inlet port to the meniscus and generate multi-material discrete or gradient structures with minimal cross-contamination. Please note that resins outside this range can also be used, however, they will exhibit a higher degree of mixing between layers. For resins used in this work, contact angles on PDMS were in the range of 55°–90°. To achieve the ideal contact angle range, high wettability areas were patterned onto the PDMS window by plasma etching (5 min; RF power-75W) with a cross-shaped mask. (Figure 2C(i–iv)). The contact angle of patterned areas was in the range of 37°–55° for all the resins tested (Figures S7, S8, Supporting Information). Plasma-etched flow paths facilitate drawing resins from greater distances and enable disruption-free, low-volume resin flow from infusion ports toward the fabrication area for multi-material MAPS with minimal cross-contamination and waste. Three distinct design configurations of PDMS window and infusion ports were tested. (Figure 2D(i-ii). While all designs worked with MAPS, the third, easy-to-clean, flat stage design with bottom port configuration was primarily used in this work.

2.3. Multi-Material Printing Using MAPS

Here, we demonstrated the versatility of MAPS printing by designing and printing a variety of multi-material structures using 2 independent infusion ports with programmable flow rates. The flat multi-port configuration was used to enable easy resin exchanges with low or no cross-contamination in both vertical and lateral directions (**Figure 3A**). For instance, "The Statue of Liberty" (Figure 3B(i); Video S3, Supporting Information), and 'a knotted vessel' geometries were printed with discrete sections of PEGDA 250 MW and PhotoCentric 3D grey resin in the vertical directions (Figure 3B(ii)). Rapid cleaning steps (Section S7, Supporting Information) were introduced between resin exchanges, and "Statue of Liberty" and "lattice cuboid" geometries were printed using PEGDA 250 MW (transparent) and commercially sourced B9Creations Black resin (black, opaque). Results show distinct layers without any contamination between layers (Figure 3C(i,ii)). Simultaneous lateral and vertical multi-material printing was demonstrated by printing an array of 3D pillars with a checkerboard roof pattern using PhotoCentric 3D grey resin and Liqcreate Composite-X resin (Figure 3C(iii)). A monolithic log-pile structure was printed with discrete sections of PEGDA 700 (top) and PEGDA 6k (bottom) (Figure 3C(iv)). PEGDA 700 (stiff, top) section retained its shape with distinct edges, while PEGDA 6k (soft, bottom) section swelled when submerged in DI water and collapsed upon drying in air. Cell-adhesive Gelatin Methacrylate (GelMA) in the form of the Syracuse University (SU) logo was printed on top of inert synthetic PEGDA 6k hydrogel using MAPS. Human osteosarcoma cells (Saos-2), seeded on the construct, were labeled for f-actin to visualize cell morphology. Results show high adhesion and spreading of cells only on GelMA regions (SU logo) while minimal-to-no cell attachment was observed on inert PEGDA 6k MW slab (Figure 3C(v)). MAPS was also used to print a 3D structure with alternating hydrophobic (PEGDA 250) and hydrophilic (PEGDA 6k) patterns forcing a water drop to travel out-of-focus along the hydrophilic line

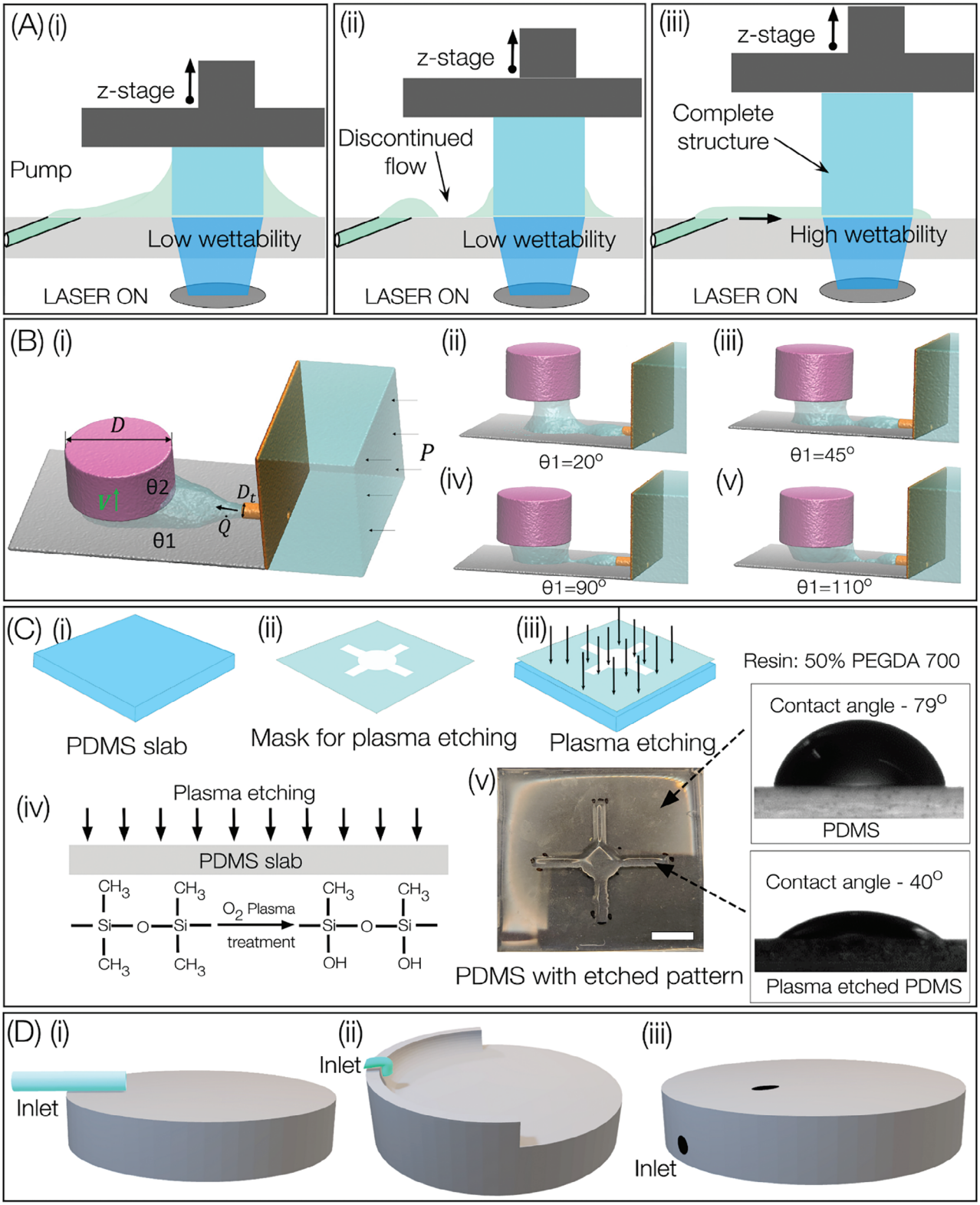

Figure 2. A) Schematics showing experimental observation of resin flow on PDMS and plasma-cleaned PDMS substrates. B) Multiphase many-body dissipative particle dynamics (mDPD) model for MAPS process with continuous infusion of new resin under varying wettability conditions. C) Process of patterning hydrophilicity on PDMS using oxygen plasma treatment, and associated changes in contact angles for 50% PEGDA 700MW resin (Scale bar –5 mm). D) Different configurations of PDMS sample holders: i) Side tube, ii) Top tube, and iii) bottom port with the slanting angle design.

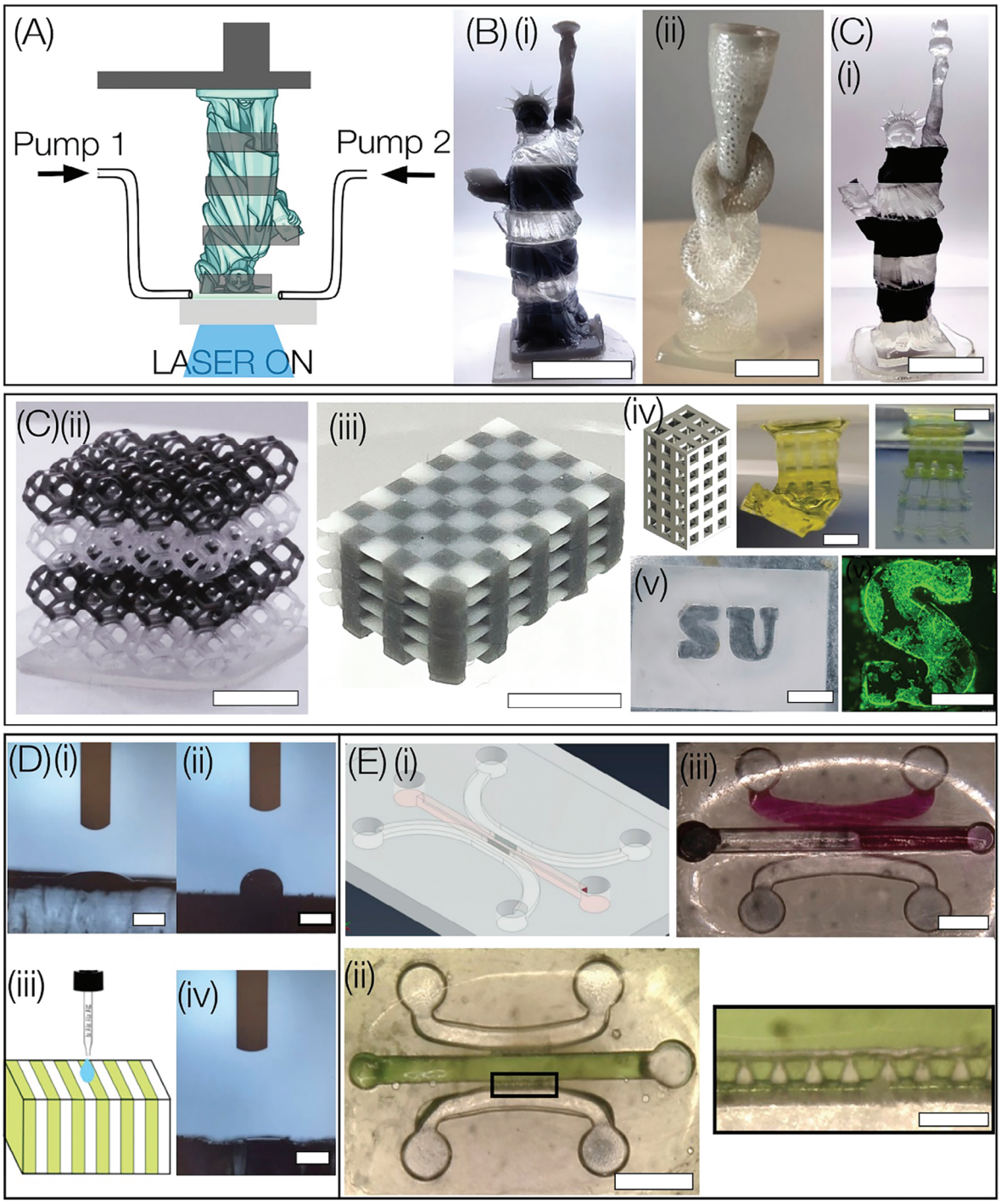

Figure 3. Multi-material printing using MAPS. A) Configuration with 2 flow pumps. B) Multi-material printing without cleaning steps: i) Statue of Liberty (scale bar –5 mm) and ii) knotted vessel printed using PEGDA 250 and PhotoCentric 3D grey resin (scale bar –5 mm), and C) with cleaning steps between resin exchanges i) Statue of Liberty printed using PEGDA 250 MW and B9Creations Black resin (scale bar –5 mm). ii, iii) Lattice cuboid and arrays of 3D pillars with checkerboard roof (scale bar –5 mm). (iv) Multi-material structure with hard (90% PEGDA 700) and soft regions (10% PEGDA 6k); only soft regions swell upon hydration and collapse when exposed to air. (Scale bar – 2 mm). (v) Multi-material printing of biologically inert (10% PEGDA 6k) and cell adhesive material (10% GelMA) (Scale bar –2 mm), with cell spreading only on GelMA (Scale bar –1 mm). D) i, ii) Contact angle formed by a water drop on flat slabs printed with PEGDA 6k, and PEGDA 250. iii) Schematic and iv) printed structure composed of alternating layers of hydrophobic (PEGDA 250) and hydrophilic (PEGDA 6k) and associated contact angle (Scale bar –1 mm). E) i) CAD design and ii) 3D printed 3-channel hydrophobic (PEGDA 250) microfluidic device with hydrophilic (PEGDA 6k) central channel separated by an array of micro-posts (scale bar –3 mm). A zoomed-in section shown by a black rectangle depicts an array of micro-posts (scale –500 µm). Green dye perfused into the central channel does not leak out into the side channels, as compared to red dye perfused into iii) an identical chip printed using a single material (PEGDA 250) (Scale bar –3 mm).

pattern, as compared to control samples (Figure 3D, Video S4, Supporting Information). Lastly, a 3-chambered microfluidic device, widely used for tissue-on-chips studies, separated by micropost arrays was printed with a central "hydrophilic" (PEGDA 6k MW) channel flanked by 2 "hydrophobic" (PEGDA 250 MW) channels using MAPS. Results show that green dye mixed in DI water remains within the central "hydrophilic" channel and does not leak into the "hydrophobic" channels. In contrast, an identical device printed only with hydrophobic resin results in leakage of dye in all channels (Figure 3E(iii)). Control over leakage in such devices can be useful for organ-on-a-chip applications.

2.4. Gradient Printing Using MAPS

To extend the capability of MAPS to print 3D structures with customized gradient properties, an inline micromixer was inserted between 2 syringe pumps and one infusion port of the PDMS window. (Figure 1A). Details related to the design, fabrication, and performance characterization of the micromixer are provided in the SI (Figures S9, S10, Video S5 (Supplementary Video)). Based on the desired gradient properties, multiple resins were mixed at defined flow rates and concentrations to generate droplets within the fabrication window. During the MAPS process, laser exposure time per layer was modulated based on mixed resin formulation. The capabilities of printing gradient complex 3D structures were assessed using a range of structures, materials, and configurations. For instance, "twisted tower" geometry with a defined color gradient (top-green, and bottom-yellow) was printed using PEGDA 700 resin (**Figure** 4A(i-ii)). Figure 4B shows the same geometry with dual property gradients (mechanical stiffness and color) using PEGDA 700 resin (brown, stiff) and PEGDA 6k resin (colorless, soft); here crosslinking times of 0.8 and 2 s were used for PEGDA 700 and PEGDA 6k for printing a layer of thickness 50 µm, while flow rates were tuned between 0–0.2 $mLmin^{-1}$ for PEGDA 700 and between 0.2 – 0 mL min^{-1} for PEGDA 6k. (Figure 4B(iii); Video S6 (Supplementary Video) Simultaneously, the exposure time was varied from 2 to 0.8 s/layer to maintain consistent curing depth even with changes in the resin formulations. The flow rates and exposure times were reversed for the structure shown in Figure 4B(ii). Section S9 (Supporting Information) provides specifics on the method used to determine the exposure time for each layer. To assess the mechanical properties of the gradient structure, different sections (≈400 µm thick) marked by black boxes in Figure 4B(ii,iv), were tested under compression. Results show that the modulus varied from 0.249 (bottom) to 3.9 MPa (top) along the height of the structure. Video S7 (Supplementary Video) shows this top-heavy gradient structure vibrates even upon gentle perturbation. To demonstrate the use of MAPS with commercially available resins, we printed gradient "Statue of Liberty" structures using a combination of PEGDA 250 (colorless) and PhotoCentric 3D grey DLP resin by linearly varying flow rates (0–0.2 mL min^{-1}). Both front and back views of the printed structure (along with associated flow rate and exposure time) are shown to highlight the uniform distribution of the resin composition achieved with this method (Figure 4C(i–iii)). We also printed the same structure with exponentially varying flow rates (Figure 4D). The modularity of choosing multiple ports, micromixers, resin flow rates, and concentrations underscores the unique capabilities of MAPS to print 3D geometries with customized gradient properties.

2.5. Gradient Printing with Additives (Magnetic Nanoparticles, Living Cells, Carbon Black)

Here, we demonstrated MAPS's capability to print 3D gradient structures with a range of additives (**Figure 5**). First, iron oxide magnetic nanoparticles (NPs) were chosen as the model NP due to their broad use in medicine, biosensing, catalysis, agriculture, and the environment.[36,37] Before performing gradient printing with NPs, processing conditions were optimized for mixed resin formulations. For instance, MAPS printing with a light intensity of 3.25 mW cm^{-2} resulted in a curing depth of 120 µm for resin with 10% NPs and an exposure time per layer of 25 s, as compared to a curing depth of 150 µm and an exposure time of 1.5 s for only resin. Optimized parameters were used to print a cylindrical geometry with a gradient structure with a maximum concentration of 10% NPs in the top section and decreasing NP concentration along the length of the cylinder. Results show that only the structures with NPs respond to the magnetic field, and the response of the gradient-aligned NPs structure (in terms of inclination angle) was distinct from that of the structure with uniform NP distribution (Figure 5A(i–iv)). The ability to incorporate other functional NPs in customized gradient configurations can be broadly applied to many applications ranging from structural colors, soft robotics, photonics, as well new patterned materials to shape electromagnetic fields.

Second, MAPS's utility for bioprinting applications is demonstrated. Although a range of bioprinting methods exist, printing structures using gradient cell densities remains challenging.[6,35,38,39] Here, MAPS was used to print a 3D structure with a gradient of cell density using a bioink composed of 5% GelMA, 4% PEGDA 6k, and 0.25% LAP, and model cells (MC3T3 pre-osteoblasts, 1 M mL^{-1}). Optimized conditions (laser power: 3.6 mW cm^{-2}; exposure time: 1 second/layer; layer thickness: 50 µm) were used to bioprint a 3D structure with gradient densities of MC3T3 along the z-direction (from top to bottom) (Figure 5B). Post-printing, the sample was washed with PBS 3 times, sliced in half, and stained for nuclei (DAPI) and f-actin, which revealed a gradient of cells with high spreading on the top section and almost no cells on the bottom (Figure 5B(iii)). 3D reconstructed confocal image of a bioprinted rectangular sample confirms the high viability of encapsulated cells and their gradient distribution from top to bottom. (Section S11, Supporting Information). A MAPS printed sample was cultured under osteogenic media for 14 days and stained with Alizarin Red to identify regions of mineral formation. Results show a gradient of mineralization from the top to the bottom section of the printed sample. (Figure 5B(iv)). These results show that MAPS can potentially generate constructs with cellular gradients for tissue engineering and regenerative medicine applications.[40,41]

Third, MAPS gradient printing was demonstrated using "carbon black", often used as an additive to reinforce the mechanical properties of 3D structures.[42,43] A cylindrical structure is printed using a PEGDA 700 and UV absorber tartrazine with defined variations in the concentration of carbon black (0%–2%)

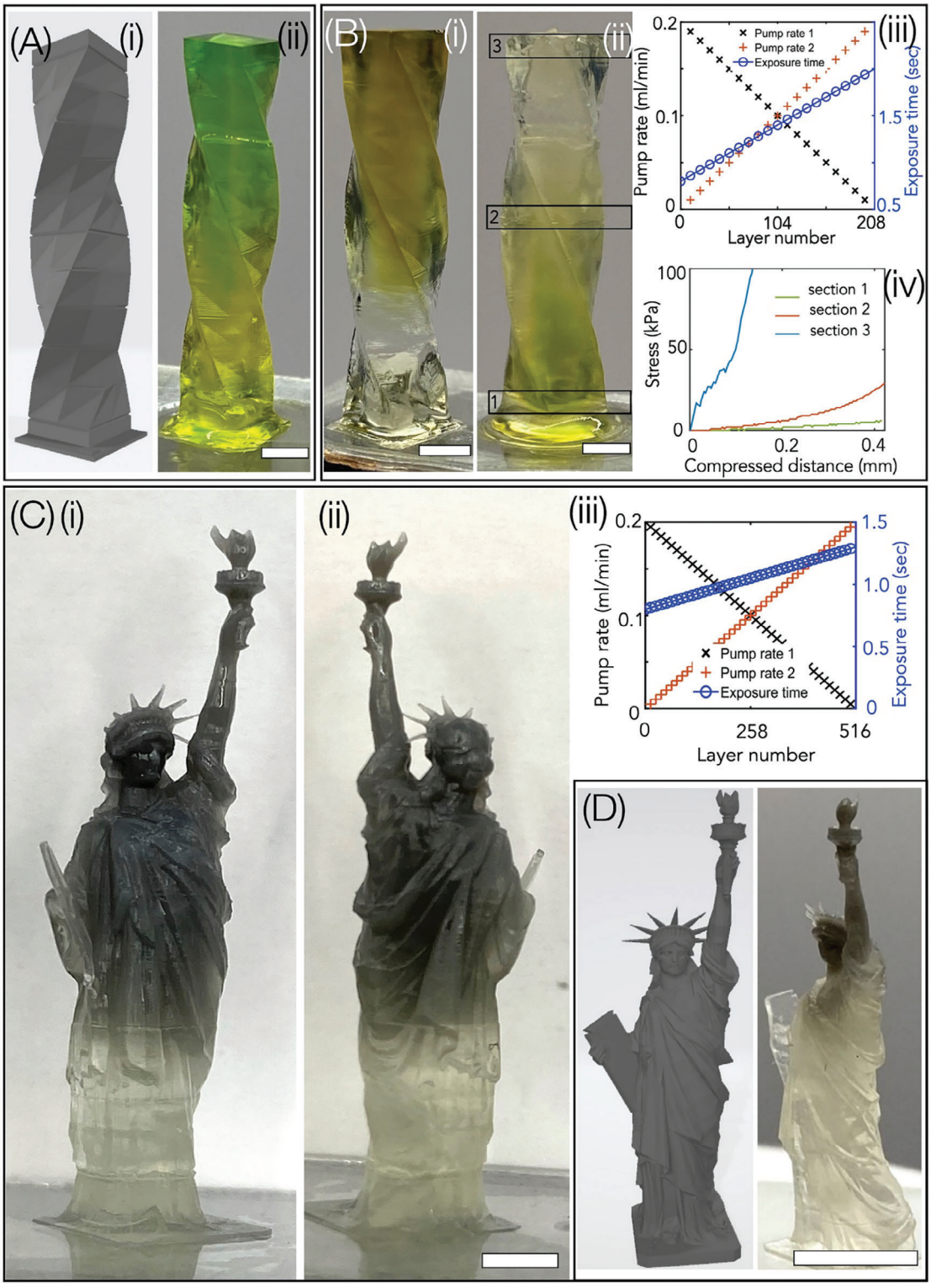

Figure 4. Gradient property printing with MAPS. A) i) displays the CAD design of the twisted tower. ii) exhibits the two-color gradient printing using green and yellow color PEGDA 700 hydrogels (scale bar – 2 mm). B) i–iii) exhibits dual color and compressive modulus gradients with PEGDA 700 and PEGDA 6k resins with associated changes in infusion flow rates and exposure times. (Scale bar – 2 mm). iv) Stress-strain plots from different sections of the printed structure (black rectangle) show that compressive modulus varies from 0.249MPa (bottom) to 3.9 MPa (top). C) i–iii) displays the front and back views of the gradient liberty tower structure printed using PEGDA 250 and photo-centric grey with associated flow rates and exposure times (scale bar – 5 mm). D) shows a CAD design of the structure (Statue of Liberty) and multi-material gradient structure with exponentially varying flow rate (Scale bar – 10 mm).

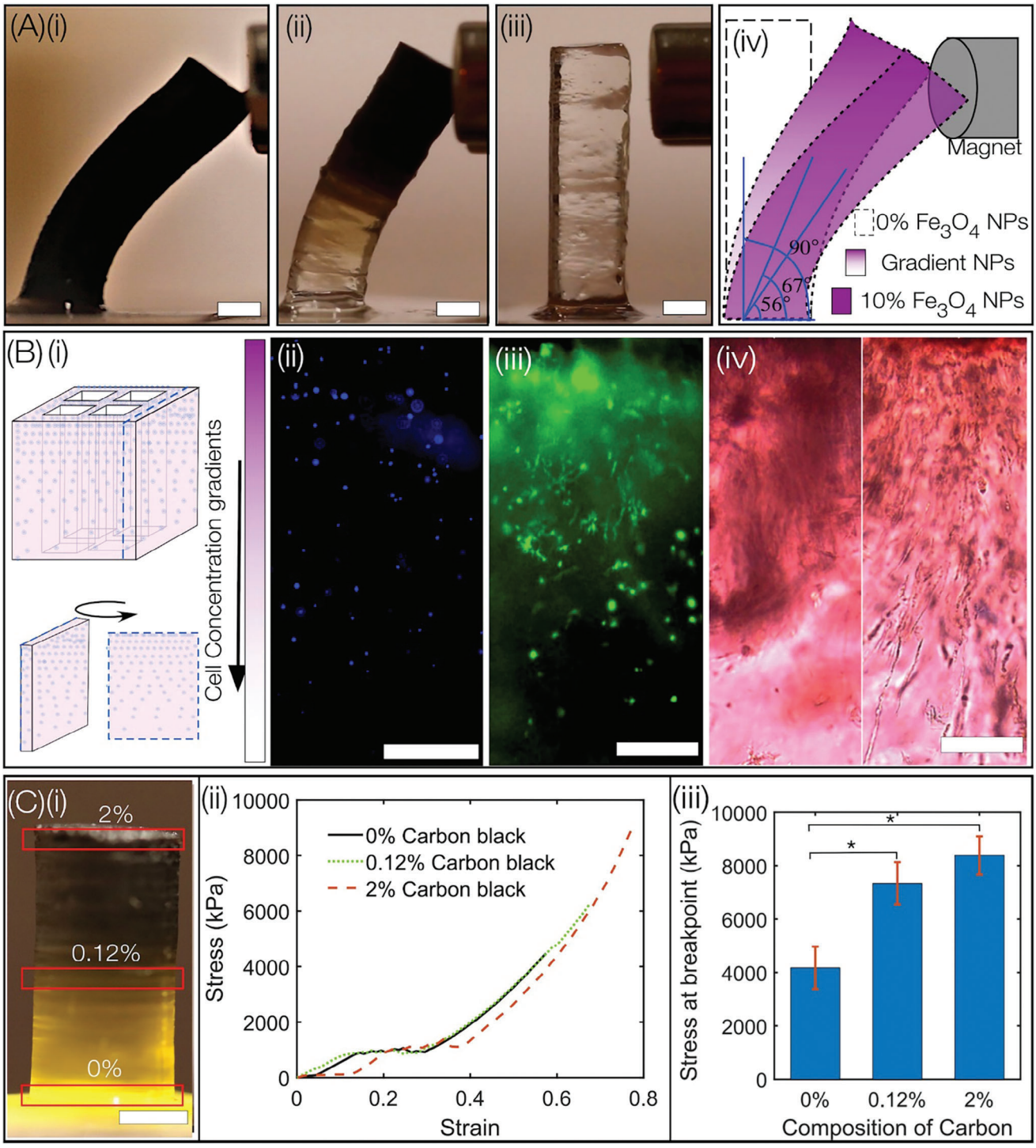

Figure 5. A) Response of cylinder geometry with i) uniformly distributed magnetic NPs, ii) gradient NPs, and iii) no NPs (control) to the magnetic field. (Scale bars −2 mm). B) i) Schematic of the bioprinted geometry with gradient cell densities along the z-direction was sliced and evaluated using various stains. ii, iii) Day 3: nuclei (blue); f-actin (green). iv) Day 14: Mineral distribution (Red). (Scale bar ii–iv) −500 µm). C) i) Cylindrical structure printed using a resin with Carbon black NPs additive (Scale bar −2 mm). ii, iii) Compressive stress-strain plot of the cylinder section marked by red rectangles, and associated stresses. (*$p < 0.0166$; error bars: mean ± SD, $n = 3$).

(Figure 5C(i)). Sections of the structure (marked by red rectangles) were compressed to obtain a compressive stress-strain plot, which shows gradient changes in breakpoint stress, from 4174 ± 793 kPa to 8385 ± 719 kPa. ANOVA test showed a p-value of 0.0037, while post hoc t-tests with Bonferroni correction showed significant differences between the 2 groups at $^{*}p < 0.0166$ demonstrating the gradient changes in the compressive modulus of the printed structure (Figure 5C(ii-iii)).

3. Discussion

MAPS is not the first vat-free 3D printing technique.[33] Droplet-DLP focuses on printing from a single resin droplet by controlling the dewetting forces to achieve optimal net utilization of resin material; here the control over resin volume within the meniscus is not important. The key innovation of our work is the programmed delivery of resin to the print window which precisely controls the volume of resin meniscus and provides control over resin formulation at a few-layer resolution; this enables printing of 3D structures with multimaterial or gradient properties not possible by droplet printing. In MAPS, a PDMS bottom window, with patterned wettability, was designed to replenish fresh resin droplets to maintain a specific volume within the print window throughout the printing process, and thus control resin composition at high resolution (50 µm/layer). Without this level of control, gradient multi-material printing of 3D structures with custom variations in mechanical stiffness, opacity, surface energy, cell densities, and magnetic properties, is not possible. Table S2 in supporting information compares MAPS with other DLP-based multi-material methods using key metrics such as scalability, resolution, control of composition per layer, cross-contamination, waste generated, and ease of use as key criteria. Key limitations of current multi-material DLP methods are also highlighted in Table S2 (Supporting Information).

4. Conclusion

We report MAPS technology and its unique ability to print complex multi-material 3D structures using a wide range of resins with minimal cross-contamination or waste, and simple materials exchange and washing protocols. MAPS distinguishes itself from other techniques like DLP-based CLIP and HARP by adopting a unique method involving the use of a planar slab instead of a VAT. This deviation yields substantial benefits in redesigning the concept of resin reservoir from VAT to meniscus formed around structure particularly advantageous when engaged in the intricate task of printing multi-material and gradient structures. We envision that MAPS will enable researchers, engineers, and innovators to push the boundaries of material science and design and fabricate custom multi-functional materials in many fields. For instance, MAPS can be used to bioprint scaffolds with gradient properties (mechanical stiffness, cell densities, cell types) to recreate the complexity of biological interfaces and tissues. Incorporation of multiple functional nanoparticles in discrete locations or in a gradient fashion at high-resolutions within 3D constructs will be useful in photonics, microelectronics, soft robotics, structural engineering, art, jewelry, and sculptures with custom material properties.

5. Experimental Section

Chemicals: ***Gelatin Methacrylate (GelMA)*** was synthesized in the laboratory. GelMA-based photopolymer was dissolved in water and mixed with **Lithium phenyl-2,4,6-trimethyl-benzoyl phosphinate (LAP)** before being this as ink. LAP was used as a photoinitiator and was synthesized in the laboratory. Please refer to SI for details on synthesis. ***PEGDA (6000 MW)*** was synthesized in the laboratory and dissolved in water and LAP was used as a photoinitiator. ***PEGDA (700 MW)*** was purchased from Sigma Aldrich, diluted in water and LAP was used as a photoinitiator. ***PEGDA (250 MW)*** and ***PEGDA (400 MW)*** were purchased from Sigma Aldrich and added with Irgacure 819 as a photoinitiator and 2-Isopropylthioxanthone (ITX) as a photosensitizer. Irgacure 819 and ITX were also purchased from Sigma Aldrich.

All of the listed commercial resins were used without further modification.

Photo resin	Manufacturer	Purchased from
Black resin	B9 creation	B9 creation
Flexible-X resin	Liqcreate	MatterHackers
Composite-X resin	Liqcreate	MatterHackers
Blu resin	Siraya Tech	Siraya Tech
Sculpt resin	Siraya Tech	Siraya Tech
eResin-Elastic resin	eSUN	MatterHackers
PhotoCentric 3D grey resin	Photocentric	MatterHackers

Optical Setup: As compared to conventional vat-based PSLA methods (Figure S1A(i), Supporting Information), vat-free MAPS is schematically depicted in Figure S1A(ii),B (Supporting Information). This approach employed a layer-by-layer additive mode of fabrication, utilizing a 405 nm laser source (Toptica) that can generate a continuous-wave (CW) laser beam with a maximum power output of 300 mW. The laser beam was directed through a diffuser (RPC Photonics Inc) to transform the Gaussian intensity distribution of the laser beam to a uniform distribution. The diffuser was mounted on a rotating mount to minimize the laser speckle generated by the diffuser. The laser beam was collimated using a convex lens and directed toward a DMD (0.95'' 1080p UV DMD, DLi Inc), which is an array of micromirrors that can be modulated to spatially pattern laser beams. The patterned laser beam was projected onto infinity-corrected projection optics, which include 2 lens systems (f = 300 mm and f = 300 mm at a distance of 60 cm). A precisely adjusted distance between the lenses focused the spatially patterned within the fabrication window. The PDMS slab was positioned above a heater (WP-16, Warner instrument) that had a hole in the center (not shown in the figure). The heater was used to warm the PDMS membrane to 40 °C for only GelMA printing, as GelMA typically gels at room temperature. The L-shaped stage and its movement were controlled using a 1D linear stage (MTS25-Z8, Thorlabs) and controller (KDC101, Thorlabs). A custom LabVIEW code was used to coordinate the alteration of the mask in the DMD with the movement of the stage in the z-direction. Additionally, 2 syringe pumps from New Era Pump Systems Inc. and a custom-designed microfluidic mixer were employed to provide a continuous supply of resin. The SyringepumpproV1 software was utilized to program the pumps during the printing of multiple materials and gradient structures.

Process Flow: The process of printing a 3D structure involves several steps. First, a CAD model was designed in Illustrator or Solid Design software. Next, MATLAB code was used to slice the 3D structure into 2D PNG images to generate a digital mask that corresponds to individual printing layers. Each image was then processed with a MATLAB code to create a 1-bit image with the desired spatial distribution for its unique 2D slice. These images were fed into a custom-written LabVIEW code that synchronized the pump flow rate, volume, upward movement of the stage, and exposure of the light pattern generated by DMD. This process ensured precise control over the printing of each layer of the 3D structure. The CAD design and dimensions of the single-channel and 4-channel sample holder

with side channel configuration are depicted (Figure S3(A–C), Supporting Information).

Contact Angle Measurement: The Contact angle was measured using a contact angle goniometer (250-F1, Rame-hart instrument co.).

Viscosity Testing: Viscosity characterization was conducted using a TA Instruments Discovery Hybrid Rheometer (DHR-3) equipped with a temperature-controlled lower Peltier plate (TA Instruments, New Castle, DE, USA). Resin viscosities were measured using a 40 mm parallel plate geometry and a flow sweep ranging from a shear rate of 0.1 to 100 s^{-1}. All viscosity measurements were carried out at 25 °C, except for resin formulations containing GelMA, which were measured at 37 °C to prevent physical gelation.

Experimental details related to the materials, hardware and software, and processing specifics.

Statistical Analysis: The error bars represent the mean ± standard deviation (SD). The statistical analysis involved variance analysis (ANOVA) with 3 independent samples per test.

Supporting Information

Supporting Information is available from the Wiley Online Library or from the author.

Acknowledgements

The authors would like to extend their thanks to Ashraf Tariq Alnatour for his assistance in programming the pump. Financial support for this project was provided by the National Institutes of Health (R21 GM141573-01) the Syracuse University Collaboration of Unprecedented Success and Excellence (CUSE) and the BioInspired Seed grant program. Work at Clemson University was supported by Artificially Intelligent Manufacturing Paradigm for Composites, an Energy Frontier Research Center, Basic Energy Sciences under Award No. DE-SC0023389 (Computation for manufacturing process optimization).

Conflict of Interest

The authors declare no conflict of interest.

Data Availability Statement

The data that support the findings of this study are available from the corresponding author upon reasonable request.

Keywords

bioprinting, digital light processing, gradient printing, meniscus, multi-material printing, nano-material printing

Received: April 27, 2024
Revised: October 27, 2024
Published online: November 15, 2024

[1] S. V. Murphy, A. Atala, *Nat. Biotechnol.* **2014**, *32*, 773.
[2] P. Kunwar, Z. Xiong, Y. Zhu, H. Li, A. Filip, P. Soman, *Adv. Opt. Mater.* **2019**, *7*, 1900656.
[3] A. J. Capel, R. P. Rimington, M. P. Lewis, S. D. R. Christie, *Nat. Rev. Chem.* **2018**, *2*, 422.
[4] N. Shahrubudin, T. C. Lee, R. Ramlan, *Procedia Manuf.* **2019**, 1286.
[5] H. Ravanbakhsh, V. Karamzadeh, G. Bao, L. Mongeau, D. Juncker, Y. S. Zhang, *Adv. Mater.* **2021**, *33*, 2104730.
[6] A. Schwab, R. Levato, M. D'Este, S. Piluso, D. Eglin, J. Malda, *Chem. Rev.* **2020**, *120*, 11028.
[7] Y. S. Zhang, G. Haghiashtiani, T. Hübscher, D. J. Kelly, J. M. Lee, M. Lutolf, M. C. McAlpine, W. Y. Yeong, M. Zenobi-Wong, J. Malda, *Nat. Rev. Methods Primers* **2021**, *1*.
[8] J. K. Placone, A. J. Engler, *Adv. Healthcare Mater.* **2018**, *7*, 1701161.
[9] S. C. Ligon, R. Liska, J. Stampfl, M. Gurr, R. Mülhaupt, *Chem. Rev.* **2017**, *117*, 10212.
[10] P. Kunwar, B. L. Andrada, A. Poudel, Z. Xiong, U. Aryal, Z. J. Geffert, S. Poudel, D. Fougnier, I. Gitsov, P. Soman, *ACS Appl. Mater. Interfaces* **2023**, *15*, 30780.
[11] J. Zhang, Q. Hu, S. Wang, J. Tao, M. Gou, *Int J Bioprint* **2020**, *6*, 211.
[12] Z. Zhao, X. Tian, X. Song, *J. Mater. Chem. C Mater.* **2020**, *8*, 13896.
[13] W. Li, M. Wang, H. Ma, F. A. Chapa-Villarreal, A. O. Lobo, Y. S. Zhang, *iScience* **2023**, *26*, 106039.
[14] P. Kunwar, A. V. S. Jannini, Z. Xiong, M. J. Ransbottom, J. S. Perkins, J. H. Henderson, J. M. Hasenwinkel, P. Soman, *ACS Appl. Mater. Interfaces* **2020**, *12*, 1640.
[15] Z. Xiong, P. Kunwar, P. Soman, *Adv. Opt. Mater.* **2021**, *9*, 2001217.
[16] Y. Wu, H. Su, M. Li, H. Xing, *J. Biomed. Mater. Res. A* **2023**, *111*, 527.
[17] U. Shaukat, E. Rossegger, S. Schlögl, *Polymers* **2022**, *14*, 2449.
[18] D. K. Patel, A. H. Sakhaei, M. Layani, B. Zhang, Q. Ge, S. Magdassi, *Adv. Mater.* **2017**, *29*, 1606000.
[19] J. T. Toombs, M. Luitz, C. C. Cook, S. Jenne, C. C. Li, B. E. Rapp, F. Kotz-Helmer, H. K. Taylor, *Science* **2022**, *376*, 1979.
[20] D. A. Walker, J. L. Hedrick, C. A. Mirkin, *Science* **2019**, *366*, 1979.
[21] J. R. Tumbleston, D. Shirvanyants, N. Ermoshkin, R. Janusziewicz, A. R. Johnson, D. Kelly, K. Chen, R. Pinschmidt, J. P. Rolland, A. Ermoshkin, E. T. Samulski, J. M. DeSimone, *Science* **2015**, *347*, 1349.
[22] C. D. Matte, M. Pearson, F. Trottier-Cournoyer, A. Dafoe, T. H. Kwok, *Rapid Prototyp J.* **2019**, *25*, 864.
[23] Q. Ge, A. H. Sakhaei, H. Lee, C. K. Dunn, N. X. Fang, M. L. Dunn, *Sci. Rep.* **2016**, *6*, 31110.
[24] A. K. Miri, D. Nieto, L. Iglesias, H. Goodarzi Hosseinabadi, S. Maharjan, G. U. Ruiz-Esparza, P. Khoshakhlagh, A. Manbachi, M. R. Dokmeci, S. Chen, S. R. Shin, Y. S. Zhang, A. Khademhosseini, *Adv. Mater.* **2018**, *30*, 1800242.
[25] D. Han, C. Yang, N. X. Fang, H. Lee, *Addit. Manuf.* **2019**, *27*, 606.
[26] B. Grigoryan, D. W. Sazer, A. Avila, J. L. Albritton, A. Padhye, A. H. Ta, P. T. Greenfield, D. L. Gibbons, J. S. Miller, *Sci. Rep.* **2021**, *11*.
[27] C. Zhou, Y. Chen, Z. Yang, B. Khoshnevis, *Rapid Prototyp J.* **2013**, *19*, 153.
[28] J. W. Choi, H. C. Kim, R. Wicker, *J. Mater. Process. Technol.* **2011**, *211*, 318.
[29] X. Li, H. Mao, Y. Pan, Y. Chen, *J. Manuf. Sci. Eng.* **2019**, *141*, 081007.
[30] G. Lipkowitz, T. Samuelsen, K. Hsiao, B. Lee, M. T. Dulay, I. Coates, H. Lin, W. Pan, G. Toth, L. Tate, E. S. G. Shaqfeh, J. M. Desimone, *Sci. Adv* **2022**, *8*, 3917.
[31] J. Cheng, R. Wang, Z. Sun, Q. Liu, X. He, H. Li, H. Ye, X. Yang, X. Wei, Z. Li, B. Jian, W. Deng, Q. Ge, *Nat. Commun.* **2022**, *13*.
[32] X. Kuang, J. Wu, K. Chen, Z. Zhao, Z. Ding, F. Hu, D. Fang, H. J. Qi, *Sci. Adv.* **2019**, *5*, 5790.
[33] Y. Zhang, Z. Dong, C. Li, H. Du, N. X. Fang, L. Wu, Y. Song, *Nat. Commun.* **2020**, *11*.
[34] K. Kowsari, B. Zhang, S. Panjwani, Z. Chen, H. Hingorani, S. Akbari, N. X. Fang, Q. Ge, *Addit. Manuf.* **2018**, *24*, 627.

[35] M. Wang, W. Li, L. S. Mille, T. Ching, Z. Luo, G. Tang, C. E. Garciamendez, A. Lesha, M. Hashimoto, Y. S. Zhang, *Adv. Mater.* **2022**, *34*, 2107038.
[36] H. V. Tran, N. M. Ngo, R. Medhi, P. Srinoi, T. Liu, S. Rittikulsittichai, T. R. Lee, *Materials* **2022**, *15*, 503.
[37] S. Gul, S. B. Khan, I. U. Rehman, M. A. Khan, M. I. Khan, *Front. Mater.* **2019**, *6*.
[38] S. Agarwal, S. Saha, V. K. Balla, A. Pal, A. Barui, S. Bodhak, *Front. Mech. Eng.* **2020**, *6*.
[39] S. You, Y. Xiang, H. H. Hwang, D. B. Berry, W. Kiratitanaporn, J. Guan, E. Yao, M. Tang, Z. Zhong, X. Ma, D. Wangpraseurt, Y. Sun, T. Lu, S. Chen, *Sci. Adv.* **2023**, *9*, 1.
[40] E. S. Bishop, S. Mostafa, M. Pakvasa, H. H. Luu, M. J. Lee, J. M. Wolf, G. A. Ameer, T. C. He, R. R. Reid, *Genes Dis.* **2017**, *4*, 185.
[41] V. Serpooshan, M. Guvendiren, *Micromachines* **2020**, *11*, 366.
[42] C. G. Robertson, N. J. Hardman, *Polymers* **2021**, *13*, 538.
[43] Y. Fukahori, *J. Appl. Polym. Sci.* **2005**, *95*, 60.